AMERICAN SOCIETY FOR MICROBIOLOGY | Antimicrobial Agents and Chemotherapy®

Structural Insights into the Mechanism of Carbapenemase Activity of the OXA-48 β-Lactamase

Clyde A. Smith,[a] Nichole K. Stewart,[b] Marta Toth,[b] Sergei B. Vakulenko[b]

[a]Stanford Synchrotron Radiation Lightsource, Stanford University, Menlo Park, California, USA
[b]Department of Chemistry and Biochemistry, University of Notre Dame, Notre Dame, Indiana, USA

ABSTRACT Carbapenem-hydrolyzing class D carbapenemases (CHDLs) are enzymes that produce resistance to the last-resort carbapenem antibiotics, severely compromising the available therapeutic options for the treatment of life-threatening infections. A broad variety of CHDLs, including OXA-23, OXA-24/40, and OXA-58, circulate in *Acinetobacter baumannii*, while the OXA-48 CHDL is predominant in *Enterobacteriaceae*. Extensive structural studies of *A. baumannii* enzymes have provided important information regarding their interactions with carbapenems and significantly contributed to the understanding of the mechanism of their carbapenemase activity. However, the interactions between carbapenems and OXA-48 have not yet been elucidated. We determined the X-ray crystal structures of the acyl-enzyme complexes of OXA-48 with four carbapenems, imipenem, meropenem, ertapenem, and doripenem, and compared them with those of known carbapenem complexes of *A. baumannii* CHDLs. In the *A. baumannii* enzymes, acylation by carbapenems triggers significant displacement of one of two conserved hydrophobic surface residues, resulting in the formation of a channel for entry of the deacylating water into the active site. We show that such a channel preexists in apo–OXA-48 and that only minor displacement of the conserved hydrophobic surface residues occurs upon the formation of OXA-48 acyl-enzyme intermediates. We also demonstrate that the extensive hydrophobic interactions that occur between a conserved hydrophobic bridge of the *A. baumannii* CHDLs and the carbapenem tails are lost in OXA-48 in the absence of an equivalent bridge structure. These data highlight significant differences between the interactions of carbapenems with OXA-48 and those with *A. baumannii* enzymes and provide important insights into the mechanism of carbapenemase activity of the major *Enterobacteriaceae* CHDL, OXA-48.

KEYWORDS antibiotic resistance, drug resistance mechanisms

Carbapenems are a class of potent β-lactam antibiotics capable of the efficient and irreversible inactivation of cell wall biosynthesis and remodeling enzymes (collectively known as the penicillin-binding proteins [PBPs]) of many clinically important bacterial pathogens. Unlike earlier β-lactams (penicillins and cephalosporins), carbapenems resist inactivation by many extended-spectrum β-lactamases (ESBLs) and thus have been used as antibiotics of last resort for the treatment of severe infections caused by ESBL-producing bacterial pathogens.

The ability of carbapenems to withstand hydrolysis by ESBLs is defined by their structural features. All β-lactam antibiotics possess a β-lactam ring fused to a second ring, with a side group on the β-lactam ring and a tail on the second ring, with both being of various sizes and structures. In the case of penicillins and cephalosporins, the second ring is either a thiazolidine or a thiazine, respectively, and the side group on the β-lactam ring is generally a large aromatic moiety linked by an amide bond (Fig. 1A and B). In carbapenems, the fused ring is a pyrroline with a sulfur atom attached externally

Citation Smith CA, Stewart NK, Toth M, Vakulenko SB. 2019. Structural insights into the mechanism of carbapenemase activity of the OXA-48 β-lactamase. Antimicrob Agents Chemother 63:e01202-19. https://doi.org/10.1128/AAC.01202-19.

Address correspondence to Clyde A. Smith, csmith@slac.stanford.edu, or Sergei B. Vakulenko, svakulen@nd.edu.

Received 14 June 2019
Returned for modification 17 July 2019
Accepted 24 July 2019
Accepted manuscript posted online 29 July 2019
Published 23 September 2019

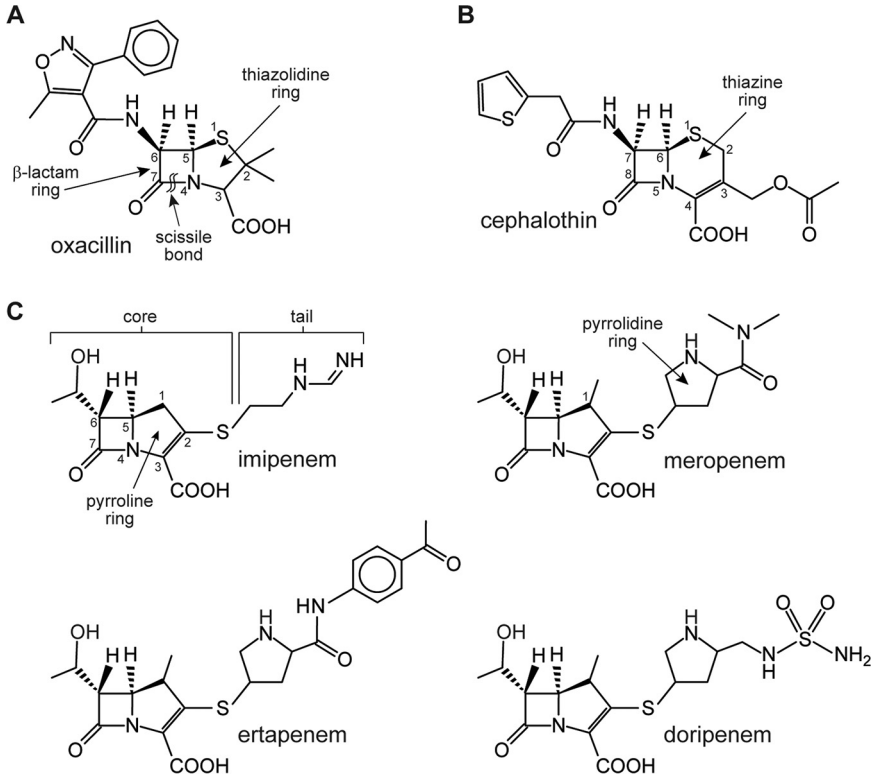

FIG 1 Chemical structures of β-lactam antibiotics. (A) Structure of the penicillin oxacillin. The β-lactam and fused thiazolidine rings are indicated, along with the atom numbering for both rings. The bond which is broken due to the activity of the β-lactamase enzymes is indicated (the scissile bond). (B) Structure of the cephalosporin cephalothin. The same β-lactam ring seen in oxacillin is present, and the fused thiazine ring is indicated, along with the atom numbering for both rings. (C) Structures of the four carbapenems used in the current study. The same β-lactam ring seen in oxacillin is present, and the fused pyrroline ring is indicated. These molecules are subdivided into the core (comprising the β-lactam, pyrroline ring, and the α-hydroxyethyl group on C-6) and the tail beyond the exocyclic sulfur atom.

at the C-2 position, which, together with the β-lactam ring, constitutes a more or less common core for all the carbapenems (Fig. 1C). The side chain on the β-lactam ring (at the C-6 carbon) is a relatively compact α-hydroxyethyl group, a distinct departure from the bulky penicillin and cephalosporin side groups (Fig. 1A and B). Unlike in the penicillins and cephalosporins, where the stereochemistry at the C-6 atom is *R*, the 6α-hydroxyethyl group of carbapenems is in the *S* configuration, and this *trans* arrangement at the C-5–C-6 bond is important for the activity and stability against hydrolysis by many β-lactamases (1, 2). The presence of the double bond in the carbapenem pyrroline ring allows for tautomerization following opening of the β-lactam upon acylation (see Fig. S1 in the supplemental material), with the C-2 atom being either sp^2 hybridized (the Δ^2 tautomer) or sp^3 hybridized (the Δ^1 tautomer). An extended tail group, which is the main point of differentiation among the various carbapenems, is linked to the exocyclic sulfur on the pyrroline ring (Fig. 1C).

Although the structural architecture of carbapenems initially protected them from hydrolysis by the majority of β-lactamases, over time an increasing number of bacteria have evolved resistance to these drugs, mainly by acquisition of novel enzymes with elevated carbapenemase activity (1). The β-lactamases are divided into four molecular classes, based on the presence of conserved amino acid motifs and amino acid sequence similarity (3, 4). Enzymes belonging to classes A, C, and D utilize an active-site serine for catalysis, while those of class B are metalloenzymes requiring zinc (5). The class A, C, and D enzymes operate through a similar two-step mechanism involving (i) the formation of a covalent acyl-enzyme intermediate following attack on the β-lactam ring by the conserved active-site serine (Fig. S1) and (ii) subsequent deacylation of the

intermediate, facilitated by a water molecule (the deacylation water) activated by a conserved glutamate, tyrosine, and lysine residue in the class A, C, and D enzymes, respectively. In the last family of enzymes, posttranslational carboxylation of the lysine residue is essential for deacylation (6). Carbapenemase activity has been observed in classes A, B, and D (7–9), including but not limited to members of the class A KPC and GES families, the class B IMP, VIM, and NDM families, and the vast OXA family of class D enzymes.

Of the class D enzymes, almost 800 have been identified in Gram-negative bacteria, with this number more than doubling in the last 5 years, along with several being recently described in some Gram-positive organisms (10, 11). The earliest discovered class D enzymes (including OXA-1, OXA-2, OXA-5, and OXA-10) were classified as narrow-spectrum β-lactamases and hydrolyzed oxacillin more efficiently than benzylpenicillin (12), hence the prevalent use of the OXA nomenclature for these enzymes. Many OXA enzyme variants with a broader spectrum of activity for β-lactams and, more alarmingly, for carbapenem antibiotics, first observed with the OXA-23 (13) and OXA-24/40 (14) enzymes of *Acinetobacter baumannii* and the OXA-48 enzyme from *Klebsiella pneumoniae* (15), have since been identified. At least 16 subfamilies of carbapenem-hydrolyzing class D β-lactamases (CHDLs), comprising 60% of all known OXA enzymes, have been identified (16). Moreover, a recent analysis has demonstrated that some of the earlier OXA β-lactamases (including OXA-2 and OXA-10) that were initially characterized as narrow- and extended-spectrum enzymes have the ability to hydrolyze carbapenems to a significant extent (17). The widespread nature of various CHDLs in *A. baumannii* (OXA-23, OXA-24/40, OXA-51, OXA-58, OXA-134, OXA-143, OXA-211, OXA-213, OXA-214, OXA-228, OXA-664, and their variants) and the OXA-48 CHDL and variants in *Enterobacteriaceae* significantly diminished the utility of carbapenems as last-resort antibiotics for the treatment of severe infections caused by these bacteria.

Over the last decade, significant progress has been made in elucidation of the mechanism of carbapenemase activity of *A. baumannii* CHDLs. Structural studies demonstrated that, unlike the earlier discovered class D β-lactamases and OXA-48 from *K. pneumoniae*, these enzymes harbor a so-called hydrophobic bridge over their active site that is involved in hydrophobic interactions with the tails of carbapenem antibiotics (18). It was also shown that the formation of the acyl-enzyme species of *A. baumannii* CHDLs with carbapenems results in the expulsion of the deacylating water molecule from the active site of these enzymes, which would prevent the next step of catalysis, deacylation, and result in inhibition. The enzymes, however, solved this problem by mobilizing one of two hydrophobic surface residues (commonly Leu and Val) juxtaposed over the active site to swing outwards to open a channel that allows a water molecule from the milieu to reach the enzymes' active site to perform deacylation (19, 20).

Unlike with *A. baumannii* CHDLs, where multiple acyl-enzyme complexes with carbapenems have been reported, no complexes were adequately described for the major *Enterobacteriaceae* CHDL, OXA-48. Structures of the apo–OXA-48 and its complexes with noncarbapenem antibiotics show that the conserved hydrophobic bridge of *A. baumannii* CHDLs is absent in OXA-48, an indication that this enzyme engages in alternative interactions with carbapenem substrates. In the absence of OXA-48–carbapenem complexes, it is also unknown whether the enzyme utilizes the same mechanism for the access of the deacylation water molecule described for *A. baumannii* CHDLs. Here we report the structures of the acyl-enzyme intermediates of the wild-type OXA-48 β-lactamase with imipenem, meropenem, ertapenem, and doripenem and present an extensive analysis of the interaction of the enzyme with these four carbapenems.

RESULTS AND DISCUSSION

Structure of OXA-48. The crystal structure of the apo form of OXA-48 was solved by molecular replacement and refined to a 1.6-Å resolution (see Fig. S2A in the supplemental material). The structure comprises the same dimer observed in all other

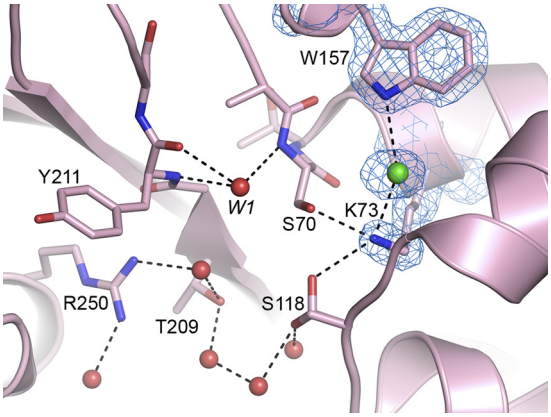

FIG 2 Final $2F_o - F_c$ density map (blue mesh, 1.0σ) for the Lys73 and Trp157 residues in apo–OXA-48 (pink ribbons). Residues involved in substrate binding and catalysis are shown as pink sticks, and their hydrogen-bonding networks are indicated by dashed lines. The chloride anion in the deacylation water pocket is shown as a green sphere in the $2F_o - F_c$ density, and the interactions that it makes with the lysine and tryptophan are shown. Water molecules that hydrogen bond to the active-site residues are shown as red spheres. Water molecule W1 is located in the oxyanion hole between Ser70 and the main chain of Tyr211.

known OXA-48 structures (21). The presence of divalent cations in the crystallization medium produces a unique crystal symmetry, where the metal ions facilitate close crystal contacts between neighboring OXA-48 dimers. Three metal binding sites were identified in the apo–OXA-48 dimer (Fig. S2A). Sites 1 and 2 both have two metal ions (one Ca^{2+} and one Cd^{2+}), and site 3 is a single Ca^{2+}.

Each independent monomer contains 243 residues (Ala23 to Pro265) folded into two distinct domains, a β-sheet domain and an α-helical domain, with the active site being sandwiched between them (Fig. S2B). A total of 256 water molecules, three Ca^{2+}, two Cd^{2+}, and three Cl^- ions complete the dimeric structure (Fig. S2A). Superposition of the two monomers gives a root mean square deviation (RMSD) of 0.19 Å for 243 matching C-α positions, and comparison with other known OXA-48 structures gives RMSD values ranging from 0.21 to 0.43 Å for the monomer and 0.26 to 0.65 Å for the dimer (Table S1). This suggests that both monomeric and dimeric structures remain essentially invariant irrespective of the crystallization conditions or whether substrates/ligands are bound.

Inspection of the electron density in the active site shows that the catalytic lysine (Lys73) is decarboxylated (Fig. 2). The side chain of Lys73 is hydrogen bonded to the O-γ atom of the catalytic serine and to a second conserved serine (Ser118), effectively blocking the site typically occupied by the deacylating water. Moreover, a chloride ion is located between the end of the Lys73 side chain and the side chain of Trp157 from the Ω loop in both monomers (Fig. 2 and Fig. S2). The active-site cleft is filled with a number of well-ordered water molecules, including one in the oxyanion hole (W1), hydrogen bonded to the amide nitrogen atoms of Ser70 and Tyr211 (Fig. 2).

Carbapenem binding. The carbapenems imipenem, meropenem, ertapenem, and doripenem were soaked into preformed OXA-48 crystals using soak times ranging from 30 s up to 10 min. Electron density maps, calculated at the shortest soak times, typically showed partial occupancy of the substrates, and soak times of 2 to 3 min were generally found to give a fully occupied complex. The initial residual electron density calculated indicated the all four acyl-enzyme intermediates were in the Δ^2 tautomeric conformation. Subsequently, all four carbapenems were built into the corresponding density and refined as the Δ^2 tautomers. The atoms making up the core of the carbapenems refined to occupancies of unity; however, the tails showed different degrees of partial occupancies of between 57 and 89%. The final $2F_o - F_c$ electron density maps (where F_o and F_c are the observed and calculated structure factor amplitudes, respectively) also showed a similar trend, with a strong connected density

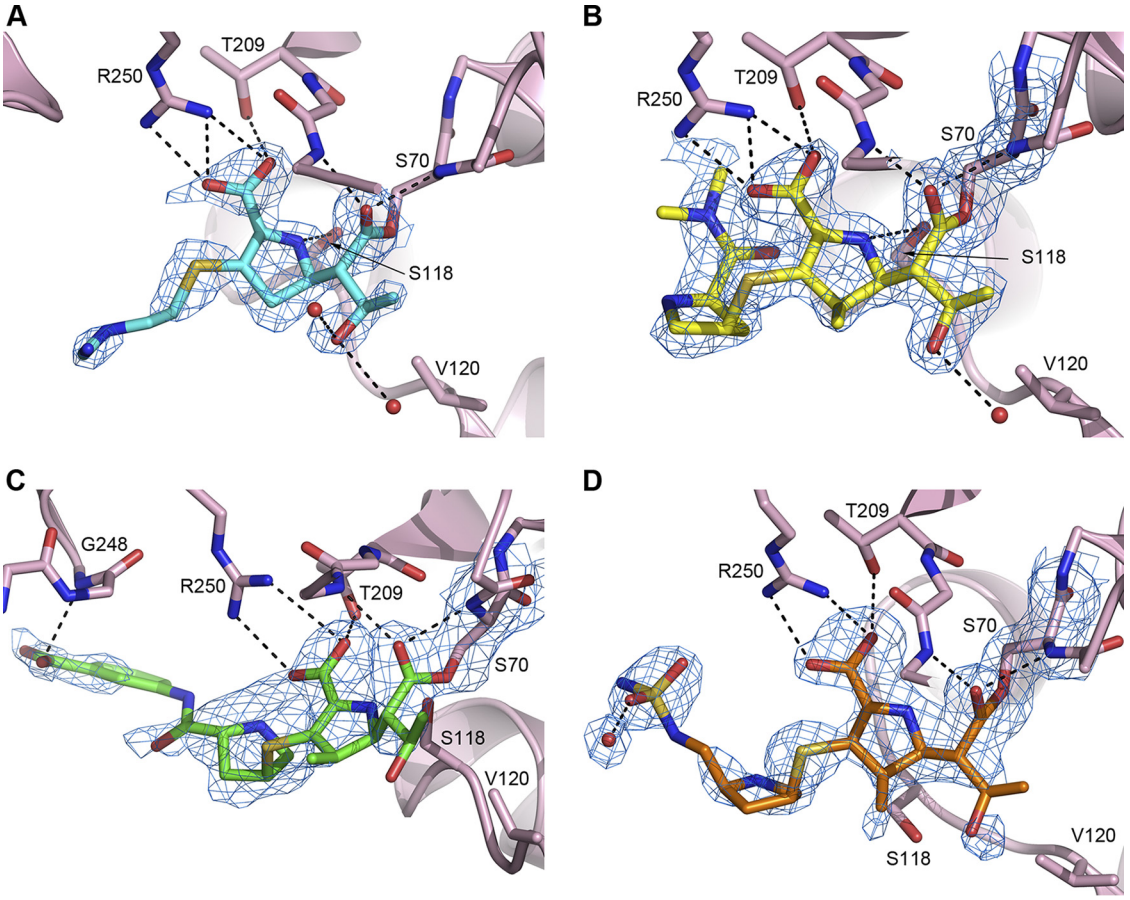

FIG 3 Final refined $2F_o - F_c$ electron density maps (blue mesh, 1.0 σ) for the carbapenems imipenem (A), meropenem (B), ertapenem (C), and doripenem (D) bound to OXA-48. The hydrogen-bonding interactions anchoring the four carbapenems in the active site of the enzyme are indicated by dashed black lines. In panels A and B, the Ser118 side chain is partially occluded behind the substrate and indicated by an arrow. Water molecules that form hydrogen-bonding interactions with the substrates are shown as small red spheres. In panel C the orientation of the complex is slightly different from that in the other three panels to show the hydrogen-bonding interaction between the ertapenem tail and Gly248 clearly. In panel D, the difference in the location of the Ser118 residue is due to a conformational difference in the loop containing Ser118 and Val120 in one of the molecules in the asymmetric unit.

for the core atoms and the exocyclic sulfur and a slightly weaker density for the tails due to structural disorder (Fig. 3). Polder omit electron density maps (22) calculated at the end of refinement (Fig. S3) confirmed the orientation of the tails of all four carbapenems.

The core of the four carbapenems is bound to OXA-48 in essentially the same orientation, interacting primarily with residues from the β-sheet domain of the enzyme. The C-7 carbonyl oxygen is anchored in the oxyanion hole, displacing the water molecule present in the apo–OXA-48 structure. The carboxylate moiety on the C-3 carbon makes an electrostatic interaction with the side chain of Arg250 at the N terminus of helix α10, a residue highly conserved in the class C and class D enzymes (10), and is further anchored by an additional hydrogen-bonding interaction with the side chain of Thr209 from strand β5, also conserved in the serine β-lactamases (Fig. 3). In the imipenem and meropenem complexes, the endocyclic nitrogen in the pyrroline ring accepts a hydrogen bond from the O-γ of Ser118, another highly conserved residue in the class D enzymes (Fig. 3A and B). This interaction is lacking for ertapenem and doripenem, due to a slight rotation of the serine side chain in these complexes (Fig. 3C and D).

In all complexes, three Cl^- ions, a Ca^{2+}, and two Cd^{2+} cations were found in the same locations as in the apo–OXA-48 dimer structure (Fig. S2). Unexpectedly, a second, nonhydrolyzed doripenem molecule was detected in the OXA-48–doripenem acyl-

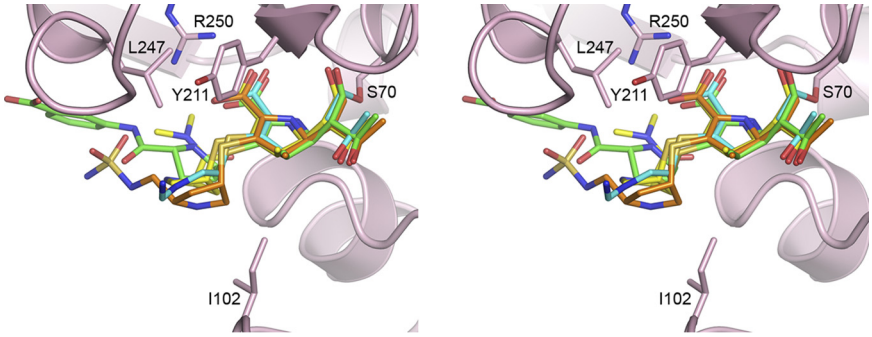

FIG 4 Stereoview of the superposition of the four OXA-48 complexes showing imipenem (cyan), meropenem (yellow), ertapenem (green), and doripenem (orange). The ribbon representation and selected side chains (pink) are shown for the imipenem–OXA-48 complexes only for clarity.

enzyme complex. The molecule is located in a shallow cleft between the C terminus of helix α10 and two surface loops connecting strands β2 and β3 and strands β6 and β7 (Fig. S4A and S4B) and is anchored in place by several hydrogen-bonding interactions with the two surface loops (Fig. S4B). None of the other three complexes show any evidence of a nonhydrolyzed substrate in the same location.

Superposition of the four carbapenem complexes onto each other and the apo–OXA-48 structure gives RMSDs of between 0.2 and 0.4 Å, with no large deviations in the positions of the active-site residues. The loops surrounding the active site (α3-α4, α4-α5, β5-β6, and the Ω loop; Fig. S2B) are not perturbed by substrate binding, adopting the same conformations in all structures. Moreover, these loops are not constrained by any crystal-packing contacts. The cores of the four substrates overlay very closely, with the tails adopting different orientations (Fig. 4), although since all four substrates are present as the Δ^2 tautomer, the tails are generally directed toward the β-strand domain. Only ertapenem has a direct interaction between the tail and the enzyme, a hydrogen bond between the terminal carboxylate group and the amide nitrogen of Gly248 (Fig. 3C); in the other three cases, there is no direct interaction, although doripenem makes a water-mediated contact (Fig. 3D). The paucity of direct and hydrophobic contacts with OXA-48 is consistent with the observed disorder in the tails of the bound carbapenems. This contrasts with the majority of known structures of imipenem, meropenem, and doripenem complexes of other OXA enzymes (listed in Table 1). In these complexes, there are either direct hydrogen-bonding interactions between the tails and the protein or hydrophobic interactions that serve to anchor the tail. The tautomerization states of the bound carbapenems in the OXA enzymes are also presented in Table 1. It is evident that there is no real consistency among the non-CHDLs (OXA-1 and OXA-13) or the CHDLs (OXA-23, OXA-24/40, OXA-48, OXA-51, and OXA-239) with respect to the tautomer state of the substrate.

The coordinates of one other OXA-48–imipenem complex are available in the Protein Data Bank (PDB) (PDB accession number 5QB4), with the interactions between the core of the substrate and enzyme being briefly described previously (23), although the tautomerization state of the pyrrolidine was not explicitly stated. Inspection of the structure and the associated electron density available on the PDB website (www.rcsb.org) shows that the acylated imipenem is built as the Δ^2 tautomer, although in two of the four molecules in the asymmetric unit, the density for the exocyclic sulfur was weak, with no density being visible for the iminoamine tail in any of the four molecules present in the asymmetric unit. Superposition of the structure with PDB accession number 5QB4 onto the imipenem–OXA-48 structure presented here gives an average RMSD of 0.3 Å (for superposition of the four molecules of the structure with PDB accession number 5QB4 onto molecules A and B of the current structure) and shows that the core of the imipenem is bound in a similar fashion in all six independent structures, with only minimal rotations of the pyrrolidine ring being seen. In three of the

TABLE 1 Carbapenem complexes of OXA enzymes

Carbapenem	Enzyme	Source	Resolution (Å)	Bridge	Tautomer	PDB accession no.
Imipenem	OXA-13	*Pseudomonas aeruginosa*	1.9	No[a]	Δ^2	1H5X
	OXA-23[b]	*A. baumannii*	1.5	No	Δ^1R	6N6U
	OXA-23[c]	*A. baumannii*	3.3	No	Δ^1R	6N6X
	OXA-48	*K. pneumoniae*	1.95	No[a]	Δ^2	5QB4
	OXA-48	*K. pneumoniae*	1.8	No[a]	Δ^2	This work
	OXA-239[d]	*A. baumannii*	1.87	Yes	Δ^1R	5WIB
Meropenem	OXA-13	*P. aeruginosa*	2.0	No[a]	Δ^2	1H8Y
	OXA-23	*A. baumannii*	2.14	Yes	Δ^1S	4JF4
	OXA-23[b]	*A. baumannii*	1.5	No	Δ^1R	6N6V
	OXA-23[c]	*A. baumannii*	3.5	No	Δ^1R	6N6Y
	OXA-48	*K. pneumoniae*	1.75	No[a]	Δ^2	This work
Ertapenem	OXA-48	*K. pneumoniae*	2.35	No[a]	Δ^2	This work
Doripenem	OXA-1	*E. coli*	1.4	No	Δ^1R	3ISG
	OXA-24/40	*A. baumannii*	2.25	Yes	Δ^2	3PAG
	OXA-24/40	*A. baumannii*	2.1	Yes	Δ^2	3PAE
	OXA-48	*K. pneumoniae*	1.9	No[a]	Δ^2	This work
	OXA-51[e]	*A. baumannii*	1.77	Yes	Δ^2	5L2F
	OXA-239[f]	*A. baumannii*	1.86	Yes	Δ^2	5WI7

[a]Both OXA-13 and OXA-48 have what is now defined as a pseudobridge rather than the classical hydrophobic bridge seen in the *A. baumannii* CHDLs.
[b]Bridge-deficient mutant, low-pH complex.
[c]Bridge-deficient mutant, neutral-pH complex.
[d]The imipenem has no tail (truncated at the sulfur) in one molecule in the asymmetric unit.
[e]The bridge residues are Phe111 and Trp222.
[f]The doripenem is truncated after the pyrrolidine ring in one molecule in the asymmetric unit.

four molecules in the structure with PDB accession number 5QB4 (molecules A, B, and C), the iminoamine tail projects in a direction opposite that observed in the current structure and makes no contacts with the protein. In molecule D, the tail configuration resembles that observed in our imipenem–OXA-48 structure, although in the structure with PDB accession number 5QB4, there is a potential hydrophobic interaction with the side chain of Tyr211 but no indication of an interaction with Ser244. These differences could result from the different crystallization conditions used to obtain the two structures and provide further confirmation that the tails of carbapenem substrates bound to OXA-48 are essentially unanchored and free to adopt multiple conformations.

The hydrophobic bridge. The hydrophobic bridge is a conserved structural feature of the *Acinetobacter* CHDLs that was originally identified in the OXA-24/40 structure and that was suggested to be responsible for the carbapenemase activity of class D β-lactamases (18). Subsequently, the bridge was found in other *A. baumannii* CHDLs. It is formed by the side chains of two conserved residues, which are located on opposite sides of the active-site cleft: one at the end of a long flexible surface loop between helices α3 and α4 and the other on the loop between strands β5 and β6 (Fig. 5A). These two residues are highly conserved in the CHDLs from *Acinetobacter* species. The residue on the long loop is predominantly phenylalanine (the OXA-24/40-like and OXA-143-like subfamilies have a tyrosine at this position). The methionine on the β5-β6 loop predominates in all CHDL subfamilies, with the exception of the OXA-213 family and the large OXA-51-like family, both of which have a tryptophan at this position.

Structural studies of acyl-enzyme complexes of various *A. baumannii* CHDLs demonstrated that the bridge spans the active site of the enzymes and is involved in hydrophobic interactions with the tails of acylated carbapenem substrates. Recently, it was also shown that the bridge can impose restrictions on the tautomeric conformation of acylated carbapenems. For carbapenems with bulky tails (such as meropenem, doripenem, and ertapenem), it allows the formation of either the Δ^1S or Δ^2 tautomer but prohibits the formation of the Δ^1R tautomer (Table 1) due to steric hindrance (24). Removal of the bridge in OXA-23 alleviates this restriction and results in the formation of the Δ^1R tautomer. Surprisingly, *A. baumannii* isolates expressing the bridge-deficient

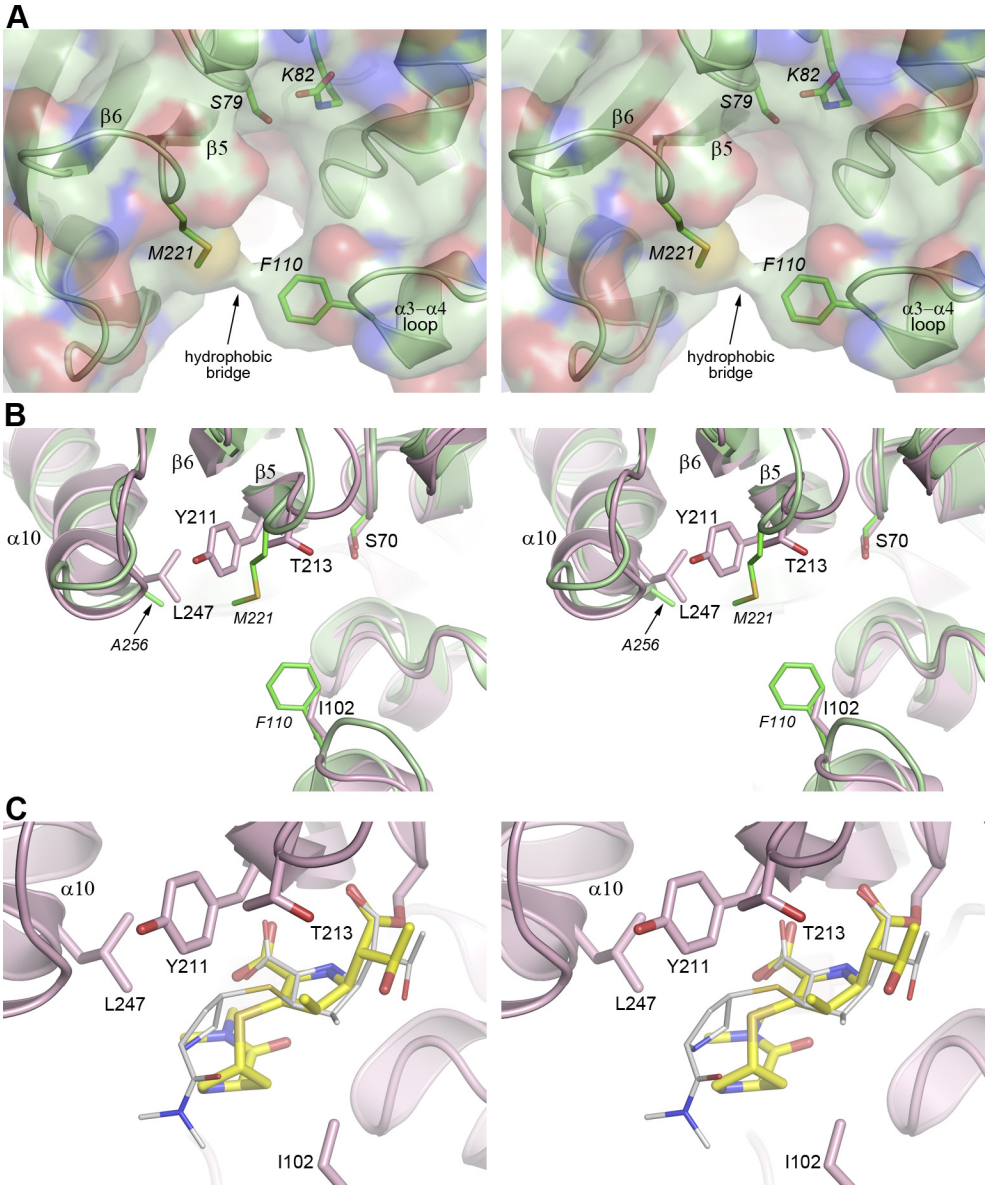

FIG 5 Stereoviews of OXA-23 and OXA-48. (A) The active site of OXA-23 (green ribbons and sticks) showing the hydrophobic bridge between Phe110 and Met221. The solvent-accessible surface of the enzyme is also shown partially transparent, and the hydrophobic contact between these two residues is evident. (B) Superposition of OXA-23 and OXA-48. The residues lining the active site are shown with the β-strand side at the top and the helical domain side at the bottom. The OXA-48 molecule is colored pink, and OXA-23 is colored green. (C) The OXA-48–meropenem complex (pink ribbons) showing the bound meropenem as the Δ^2 tautomer in yellow. The Δ^1R meropenem tautomer from the bridge-deficient OXA-23 mutant complex is shown as thin gray sticks.

mutant still produced resistance to carbapenems, albeit at lower levels (24), an indication that the bridge is only partially responsible for the carbapenemase activity of the enzyme. This seems entirely consistent with the finding that OXA-48, OXA-2, and OXA-10 (which also lack an OXA-23- or OXA-24/40-type hydrophobic bridge) possess carbapenemase activity equal to that of some known *A. baumannii* CHDLs (17).

The OXA-48 enzyme does not possess the same hydrophobic bridge described for the CHDLs from *Acinetobacter*. The corresponding residues in OXA-48 are an isoleucine (Ile102) and a threonine (Thr213) (Fig. 5B), and analysis of the sequences of the other non-*Acinetobacter* CHDL subfamilies shows that both isoleucine and threonine predominate in these positions. Superposition of OXA-48 and OXA-23 shows that both the long α3-α4 loop and the β5-β6 loop are essentially isostructural in these two enzymes.

While the Phe110 and Met221 side chains in OXA-23 are close enough (approximately 4 Å of separation) to form a bridge, the equivalent residues in OXA-48 are separated by over 9.5 Å (Fig. 5B).

In the absence of a bridge in OXA-48, all four acyl-enzyme complexes of carbapenems are in the Δ^2 tautomeric conformation. To investigate whether the two stereoisomers of the Δ^1 tautomer can also be accommodated by OXA-48, we superimposed the structures of the wild-type and the bridge-deficient OXA-23 Δ^1S and Δ^1R meropenem complexes, respectively, onto the active site of the OXA-48–meropenem complex (19, 24). While there was no impediment to the formation of the Δ^1S tautomer, a severe steric clash with Tyr211 was observed with the Δ^1R tautomer (Fig. 5C). In OXA-48, the side chain of Tyr211 occupies a position more or less equivalent to Met221 in OXA-23, and this is facilitated by a sequence difference at the N terminus of the adjacent α10 helix. In the majority of the *Acinetobacter* CHDLs, the first residue of helix α10 is an alanine (Ala256 in OXA-23; Fig. 5B), whereas in the non-*Acinetobacter* enzymes, this is predominantly a larger hydrophobic residue, such as an isoleucine, leucine, or methionine (Leu247 in OXA-48; Fig. 5B). The extra bulk of this residue in OXA-48 forces the Tyr211 to adopt a conformation where it has rotated out into the active-site cleft. Although a classical hydrophobic bridge, as described for the *Acinetobacter* CHDLs, does not form in OXA-48, the Tyr211 side chain could be deemed a pseudobridge, in that it does seem to prevent the formation of the Δ^1R tautomer, similar to what has been observed with the classical bridge of *A. baumannii* CHDLs.

The deacylating water channel. A key feature of the mechanism of action of the OXA enzymes is the requirement for the posttranslational carboxylation of Lys73, located in the active site adjacent to the catalytic serine. The carboxylate group is responsible for the activation of a water molecule, which then attacks the acyl bond of the intermediate and leads to deacylation and release of the inactivated substrate (6). The carboxylated lysine is shielded from the external solvent by a hydrophobic patch formed by two conserved juxtaposed aliphatic residues from the Ω loop on one side (Leu166 in OXA-23, for example) and the α4-α5 loop on the other (Val128 in OXA-23). It has been suggested that the *A. baumannii* CHDLs gained the ability to deacylate carbapenem acyl-enzyme intermediates by opening a channel into the vicinity of the carboxylated lysine via the movement of the aliphatic residues that form the hydrophobic patch (19, 20). In these enzymes, this channel opens as a direct consequence of the binding of a carbapenem substrate. Upon acylation, the 6α-hydroxyethyl group pushes against the two juxtaposed hydrophobic residues. This steric interaction forces one of these residues to adopt a different rotameric form, and as a consequence, the transient water channel is opened.

Comparison of the apo form and carbapenem-bound structures of OXA-48 shows that although the same pairing of juxtaposed aliphatic residues (Val120 and Leu158) exists, there is no severe steric hindrance with the acylated antibiotic. Analysis of the solvent-accessible surface of the apo–OXA-48 structure suggests that unlike in the apo forms of the *A. baumannii* CHDLs (Fig. S5A and B), where the surface is fully closed over the lysine, in apo–OXA-48 there is a preexisting channel between the hydrophobic patch and the catalytic serine (Fig. 6A), which leads directly into a cavity occupied by the chloride ion bound between Lys73 and Trp157 (Fig. 6B). Formation of the acyl-enzyme intermediate of OXA-48 causes just minor localized movements of the conserved Val120 and Leu158 residues, which slightly widens the preexisting channel to allow for the ingress of a water molecule into the vicinity of the deacylating water pocket (Fig. 6C to F).

This is in contrast to what was observed in OXA-23 (19), where the surface between the hydrophobic patch (formed by Val128 and Leu166) and the catalytic serine is closed in the apo form of the enzyme (Fig. S5A), and it is not until meropenem binds that the Leu166 residue is pushed away by the 6α-hydroxyethyl group to open a transient channel for water ingress. A similar analysis of the solvent-accessible surface of OXA-24/40 (Fig. S5B) also shows that in this enzyme the hydrophobic patch (formed by

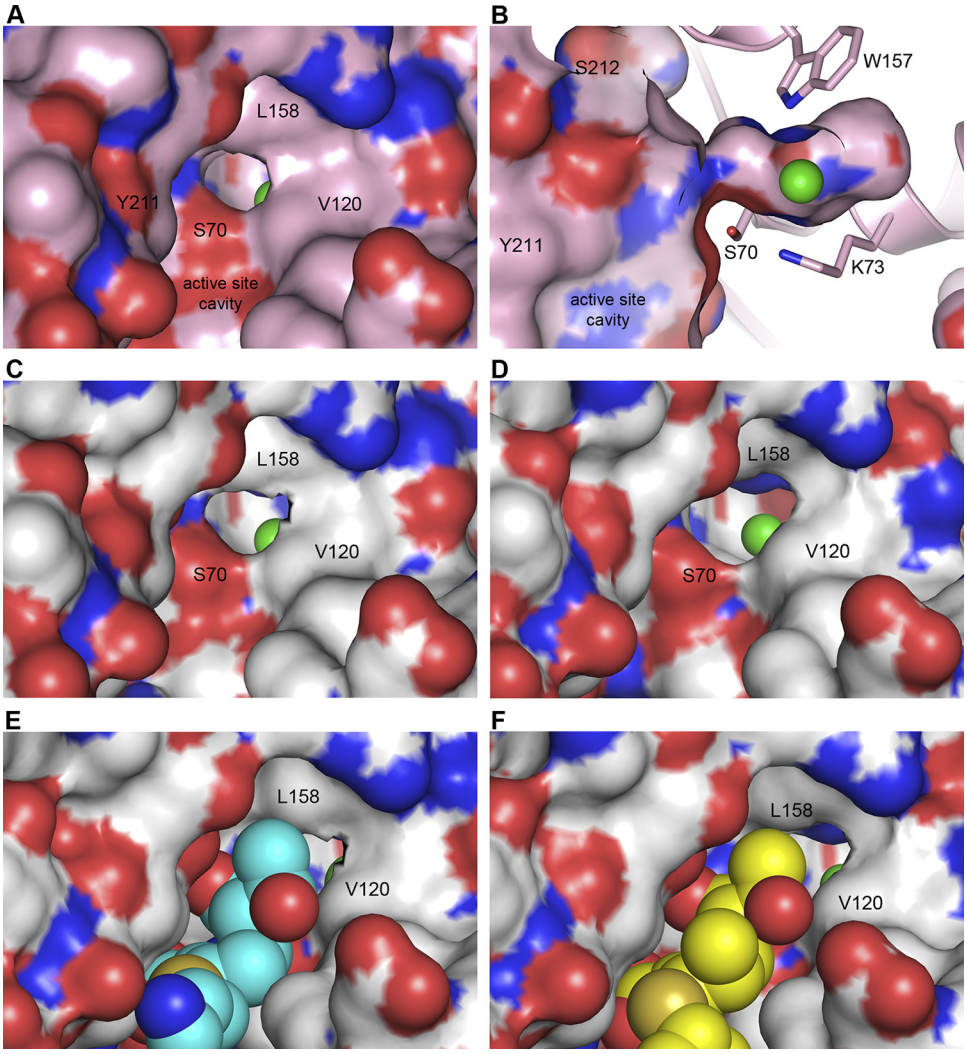

FIG 6 Solvent-accessible surfaces. (A) The surface calculated for apo–OXA-48 (pink) in the active site, using a probe radius of 1.4 Å. The juxtaposed hydrophobic residues (Leu158 and Val120) are indicated, and the channel between these residues and the Ser70 side chain is observed. The bound chloride anion (green sphere) can just be seen through the channel. (B) The apo–OXA-48 surface rotated 90° relative to the structure in panel A. The channel between the active-site cavity and the pocket containing the chloride (which occupies the position of the carboxylate in the carboxylated lysine, if it is present) is evident. (C) The surface calculated for imipenem–OXA-48 (gray) showing the channel and the chloride anion (green). The imipenem substrate is not shown. (D) The surface calculated for meropenem–OXA-48 (gray) showing the channel and the chloride anion (green). The meropenem substrate is not shown. (E) The same as panel C with the bound imipenem shown as cyan close-packed spheres. The opening to the deacylation pocket is still accessible. (F) The same as panel D with bound meropenem (yellow CPK), with the channel into the deacylation pocket still being accessible.

Val130 and Leu168) is closed over the deacylation water pocket, and when doripenem binds, the valine side chain is forced to rotate to accommodate the 6α-hydroxyethyl and, in so doing, opens the transient water channel (Fig. S5C and D).

The movement of the hydrophobic residues in CHDLs upon carbapenem acylation can be quantified by superimposing their apo- and acyl-enzyme structures. In OXA-23, such superposition places the C-9 carbon atom of the 6α-hydroxyethyl group of the acylated substrate only 2.4 Å from the C-δ2 atom of the Leu166 side chain (Fig. 7A). This distance is significantly shorter than the van der Waals contact distance for two nonbonded carbon atoms of 3.2 to 3.3 Å (25), which would give rise to a severe steric clash. To relieve this clash, either the bound meropenem would be forced to bind in a suboptimal way or a large conformational change of the leucine side chain would have to occur to accommodate the 6α-hydroxyethyl. Indeed, it is the latter that is observed

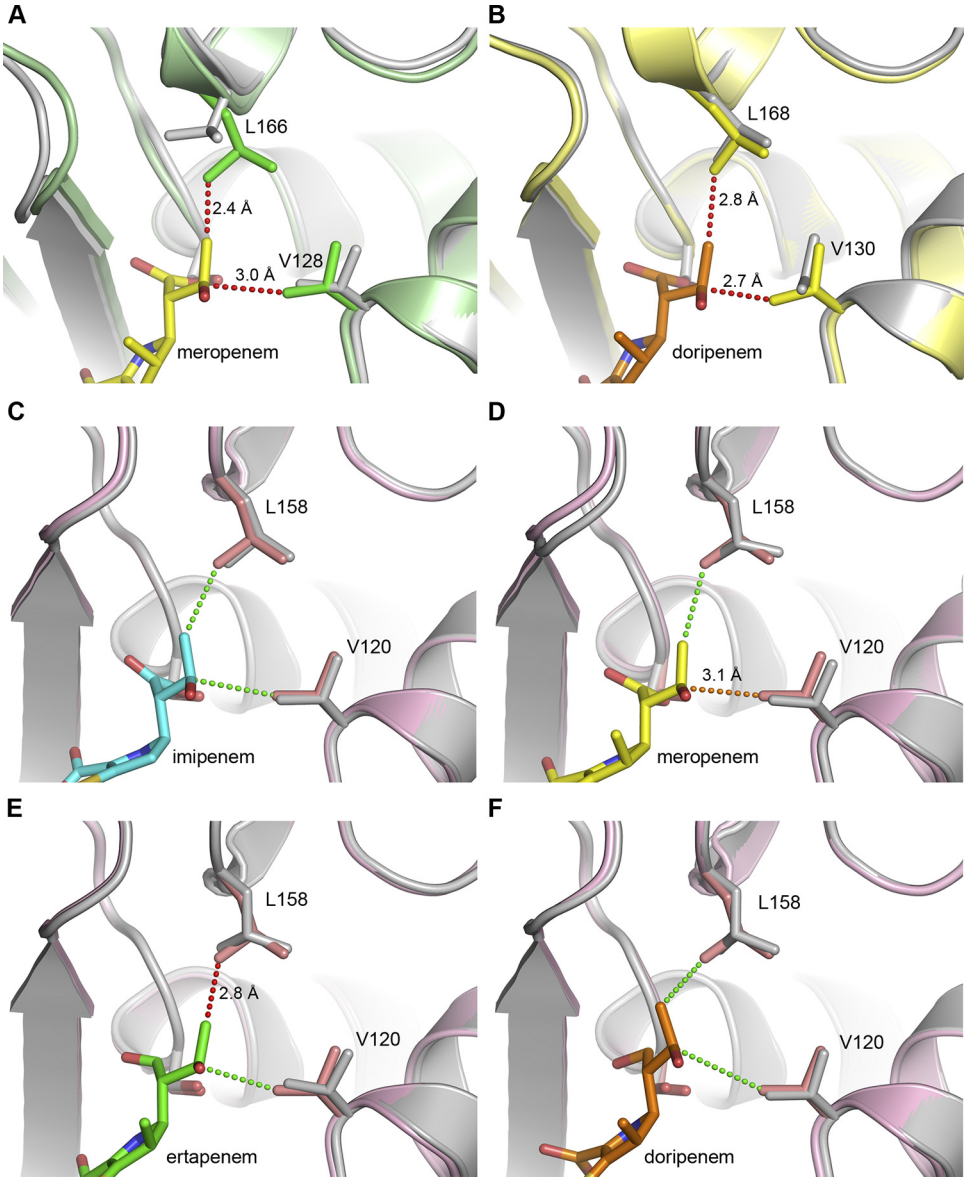

FIG 7 The active sites of the *A. baumannii* CHDLs. (A) Superposition of the meropenem complex of OXA-23 (gray ribbons and sticks) onto apo–OXA-23 (green ribbons and sticks). The two juxtaposed hydrophobic residues (Leu166 and Val128) are indicated for both structures. The closest nonbonded contacts between meropenem and the residues in the apo–OXA-23 structure are indicated. (B) Superposition of the doripenem complex of OXA-24/40 (gray ribbons and sticks) onto apo–OXA-24/40 (yellow ribbons and sticks). The two juxtaposed hydrophobic residues (Leu168 and Val130) are indicated for both structures. The closest nonbonded contacts between doripenem and the residues in the apo–OXA-24/40 structure are indicated. (C) Superposition of imipenem–OXA-48 (gray) onto apo–OXA-48 (pink). (D) Superposition of meropenem–OXA-48 (gray) onto apo–OXA-48 (pink). (E) Superposition of ertapenem–OXA-48 (gray) onto apo–OXA-48 (pink). (F) Superposition of doripenem–OXA-48 (gray) onto apo–OXA-48 (pink). The close contacts are shown as dotted lines and colored green if the distance is >3.2 Å, orange (D) when the distance is 3.1 Å, and red (E) when the distance is less than 3 Å.

in this enzyme complex (19), where the leucine side chain transitions by 2.2 Å into an alternative rotameric form, which increases the distance between the 6α-hydroxyethyl and the leucine side chain to 4.2 Å. There is also a minor movement of the α4-α5 loop carrying the valine side chain (Fig. 7A) to alleviate a minor steric clash (3.0 Å) between the C-8 atom and the C-γ2 atom of the valine, but the rotameric form of the valine is retained. In OXA-24/40, similar measurements indicate that the distance from C-8 to valine C-γ2 is now the shortest one (at 2.7 Å), and the clash here is relieved by a transition of the valine into an alternate rotameric form, where the shortest distance is

now 3.8 Å. There is also a concomitant small translation of the leucine residue (by about 0.4 Å) away from the substrate (Fig. 7B). This is consistent with the simultaneous presence of both valine rotamers in the related enzyme OXA-143 (20), which suggests a reasonably low energy barrier between the two rotameric forms.

Unlike in the *A. baumannii* CHDLs, in OXA-48 the corresponding nonbonded contacts between the carbapenems and the Leu158 and Val120 side chains are longer (approximately 3.3 to 3.4 Å, on average) and do not result in steric clashes between the 6α-hydroxyethyl and the two juxtaposed hydrophobic residues. There are, however, some small movements (Fig. 7C to F). In all cases, there is a minor outward movement of the α4-α5 loop, and consequently, the Val120 side chain also moves (by approximately 0.1 to 0.2 Å). In the meropenem, ertapenem, and doripenem complexes, the isobutyl side chain of Leu158 rotates 180° about the C-β–C-γ bond so that the C-δ1 and C-δ2 atoms point in the opposite direction, increasing the contact distance by about 0.1 to 0.2 Å. Only one of these complexes (ertapenem) has a closest approach distance (2.8 Å) less than the carbon-carbon nonbonded van der Waals distance (Fig. 7E), while the meropenem and doripenem complexes both have closest contact distances greater than 3.2 Å (Fig. 7D and F). It is therefore not understood why there has been a flip of the leucine residue in these two complexes. Only the imipenem complex has the same leucine rotamer as the apo–OXA-48 form (Fig. 7C). This seems to be an important distinction between OXA-48 and the *A. baumannii* CHDLs, in that these minor movements of the leucine and valine residues upon carbapenem binding to OXA-48 serve to slightly widen the preexisting deacylation water channel, whereas in the *A. baumannii* enzymes, large-scale changes are necessary to create the channel in the first place.

Irrespective of whether the channel is open permanently (as in OXA-48) or is transient in response to carbapenem binding (as in the *A. baumannii* enzymes), it is clearly an important feature of the CHDLs. Deacylation of the covalent intermediate cannot occur if a water molecule is unable to enter into the vicinity of the acyl bond to be activated by the carboxylated lysine, and enzymes that cannot achieve this deacylation step are effectively inhibited by carbapenem substrates. The CHDLs have evolved the ability to deacylate a covalently bound carbapenem not by undergoing macroscopic changes to their structure but, rather, by small relative movements of the loops containing the two juxtaposed hydrophobic residues or by providing the space to allow the hydrophobic residues to adopt alternate rotameric conformations.

MATERIALS AND METHODS

Protein purification. For the large-scale purification of OXA-48, its gene was cloned into the pET24a(+) expression vector without the 63 nucleotides encoding the 21-amino-acid N-terminal leader peptide. The recombinant plasmid was introduced into *Escherichia coli* BL21(DE3), and the expression of OXA-48 was induced by addition of isopropyl-β-D-thiogalactopyranoside (IPTG) to a final concentration of 1 mM. The enzyme was purified as described previously (17), with some modifications. Briefly, *E. coli* cells were harvested by centrifugation, the intracellular enzyme was liberated by sonication, and the supernatant was passed through a High Q anion-exchange column. OXA-48 was collected from the flowthrough fractions, concentrated, and dialyzed against 25 mM HEPES, pH 7.5, buffer. The enzyme was subsequently loaded on a High S cation-exchange column and eluted with NaCl (0 to 0.5 M). Fractions containing OXA-48 were dialyzed against 25 mM HEPES, pH 7.5, buffer, concentrated to 3 mg/ml, and stored at 4°C. The protein was more than 95% pure, as judged by SDS-PAGE. We measured its activity with doripenem (data not shown) and found that the enzyme had the same activity previously reported (17).

Crystallographic analysis of OXA-48–carbapenem complexes. Crystals of OXA-48 were grown under multiple conditions using PEG/Ion and PEG/Ion-2 screens (Hampton Research), in addition to the original published conditions (0.1 M HEPES, pH 7.5, 8% butanol, 10% polyethylene glycol [PEG] 8000). Several of these conditions had pH values of 6 or below or were unbuffered and were deemed to be good options for soaking experiments with carbapenem substrates. Subsequent diffraction analysis showed that the variation in conditions gave rise to a similar variation in the space group and unit cell and a range of resolution limits (see Table S2 in the supplemental material). Comparison of these conditions and crystallographic parameters with published conditions for OXA-48 also showed a wide variation in crystallographic parameters and no real consistency, with the exception of the crystals produced when the enzyme was crystallized in the presence of divalent cations (26, 27). Condition 42 from the PEG/Ion-2 screen contains 5 mM each $CaCl_2$, $CoCl_2$, and $CdCl_2$ (along with 20% PEG 3350) and gives crystals in $P2_12_12_1$ with cell dimensions of $a = 70.8$ Å, $b = 76.8$ Å, and $c = 100.1$ Å, which diffract to a 1.6-Å resolution. Although unbuffered, the pH of the condition was measured at be about 4. This condition was chosen for subsequent soaking experiments.

A diffraction data set to a 1.6-Å resolution was collected from a single apo-crystal at Stanford Synchrotron Radiation Lightsource (SSRL) beamline BL12-2, using X rays at 12,658 eV (0.9795 Å). A total of 1,800 images were collected with a Pilatus 6M PAD detector, with each image comprising a 0.2° rotation. The images were processed with the XDS program package (28) and scaled/merged with the AIMLESS program (29). Data collection statistics are given in Table S3. The structure was solved by molecular replacement (MR) with the program MOLREP (30), using the refined apo–OXA-48 structure (PDB accession number 4S2P) (31). The models were manually rebuilt using the COOT program (32) and refined with the PHENIX.REFINE program (33). Refinement statistics are given in Table S4. The polder omit $F_o - F_c$ densities (22) for the four carbapenems, calculated at the end of refinement, are shown in Fig. S3.

Carbapenem complexes were prepared by soaking preformed apo–OXA-48 crystals in modified crystallization buffer supplemented with cryoprotectant (25% glycerol) and 50 mM the four carbapenem substrates (imipenem, meropenem, doripenem, and ertapenem). The crystals were soaked for various times ranging from 30 s to 10 min and then flash-cooled in liquid nitrogen prior to diffraction screening and data collection. Diffraction data were collected from the soaked crystals at SSRL beamline BL12-2 using X rays at 12,658 eV (0.9795 Å). Data collection statistics are given in Table S3. All structures were solved by molecular substitution using the refined apo–OXA-48 structure. Acylated carbapenem substrates were built into the residual electron density in the active site using the COOT program (32), and the structures, including the occupancies of the bound substrates, were refined with the PHENIX.REFINE program (33). Refinement statistics are given in Table S4.

Data availability. The coordinates and structure factors for the OXA-48 structures used in this study have been deposited in the Protein Data Bank (http://www.rcsb.org/) with the following accession numbers: 6P96 for the complex with the apo form, 6P97 for the imipenem complex, 6P98 for the meropenem complex, 6P99 for the doripenem complex, and 6P9C for the ertapenem complex.

SUPPLEMENTAL MATERIAL

Supplemental material for this article may be found at https://doi.org/10.1128/AAC.01202-19.

SUPPLEMENTAL FILE 1, PDF file, 0.9 MB.

ACKNOWLEDGMENTS

This work is supported by a grant from the National Institutes of Health (grant R01AI114668 to S.B.V.). Portions of this research were carried out at the Stanford Synchrotron Radiation Lightsource (SSRL). Use of SSRL is supported by the U.S. Department of Energy, Office of Science, Office of Basic Energy Sciences, under contract no. DE-AC02-76SF00515. The SSRL Structural Molecular Biology Program is supported by the DOE Office of Biological and Environmental Research and by the National Institutes of Health (NIH), National Institute of General Medical Sciences (NIGMS) (including grant P41GM103393).

The contents of this publication are solely the responsibility of the authors and do not necessarily represent the official views of NIGMS or NIH.

REFERENCES

1. Papp-Wallace KM, Endimiani A, Taracila MA, Bonomo RA. 2011. Carbapenems: past, present, and future. Antimicrob Agents Chemother 55:4943–4960. https://doi.org/10.1128/AAC.00296-11.
2. Zhanel GG, Wiebe R, Dilay L, Thomson K, Rubinstein E, Hoban DJ, Noreddin AM, Karlowsky JA. 2007. Comparative review of the carbapenems. Drugs 67:1027–1052. https://doi.org/10.2165/00003495-200767070-00006.
3. Ambler RP. 1980. The structure of β-lactamases. Philos Trans R Soc Lond B Biol Sci 289:321–331. https://doi.org/10.1098/rstb.1980.0049.
4. Ambler RP, Coulson AFW, Frere JM, Ghuysen JM, Joris B, Forsman M, Levesque RC, Tiraby G, Waley SG. 1991. A standard numbering scheme for the class-A β-lactamases. Biochem J 276:269–270. https://doi.org/10.1042/bj2760269.
5. Leonard DA, Bonomo RA, Powers RA. 2013. Class D β-lactamases: a reappraisal after five decades. Acc Chem Res 46:2407–2425. https://doi.org/10.1021/ar300327a.
6. Golemi D, Maveyraud L, Vakulenko S, Samama JP, Mobashery S. 2001. Critical involvement of a carbamylated lysine in catalytic function of class D β-lactamases. Proc Natl Acad Sci U S A 98:14280–14285. https://doi.org/10.1073/pnas.241442898.
7. Meletis G. 2016. Carbapenem resistance: overview of the problem and future perspectives. Ther Adv Infect Dis 3:15–21. https://doi.org/10.1177/2049936115621709.
8. Queenan AM, Bush K. 2007. Carbapenemases: the versatile β-lactamases. Clin Microbiol Rev 20:440–458. https://doi.org/10.1128/CMR.00001-07.
9. Codjoe FS, Donkor ES. 2018. Carbapenem resistance: a review. Med Sci (Basel) 6:1–28. https://doi.org/10.3390/medsci6010001.
10. Toth M, Antunes NT, Stewart NK, Frase H, Bhattacharya M, Smith CA, Vakulenko SB. 2016. Class D β-lactamases do exist in Gram-positive bacteria. Nat Chem Biol 12:9–14. https://doi.org/10.1038/nchembio.1950.
11. Toth M, Stewart NK, Smith C, Vakulenko SB. 2018. Intrinsic class D β-lactamases of *Clostridium difficile*. mBio 9:e01803-18. https://doi.org/10.1128/mBio.01803-18.
12. Fisher JF, Meroueh SO, Mobashery S. 2005. Bacterial resistance to β-lactam antibiotics: compelling opportunism, compelling opportunity. Chem Rev 105:395–424. https://doi.org/10.1021/cr030102i.
13. Paton R, Miles RS, Hood J, Amyes SGB, Miles RS, Amyes SGB. 1993. ARI-I: β-lactamase-mediated imipenem resistance in *Acinetobacter baumannii*. Int J Antimicrob Agents 2:81–88. https://doi.org/10.1016/0924-8579(93)90045-7.
14. Bou G, Oliver A, Martinez-Beltran J. 2000. OXA-24, a novel class D β-lactamase with carbapenemase activity in an *Acinetobacter baumannii* clinical strain. Antimicrob Agents Chemother 44:1556–1561. https://doi.org/10.1128/AAC.44.6.1556-1561.2000.
15. Poirel L, Héritier C, Tolün V, Nordmann P. 2004. Emergence of oxacillinase-mediated resistance to imipenem in *Klebsiella pneumoniae*. Antimicrob Agents Chemother 48:15–22. https://doi.org/10.1128/aac.48.1.15-22.2004.
16. Evans BA, Amyes SG. 2014. OXA β-lactamases. Clin Microbiol Rev 27:241–263. https://doi.org/10.1128/CMR.00117-13.

17. Antunes NT, Lamoureaux TL, Toth M, Stewart NK, Frase H, Vakulenko SB. 2014. Class D β-lactamases: are they all carbapenemases? Antimicrob Agents Chemother 58:2119–2125. https://doi.org/10.1128/AAC.02522-13.
18. Santillana E, Beceiro A, Bou G, Romero A. 2007. Crystal structure of the carbapenemase OXA-24 reveals insights into the mechanism of carbapenem hydrolysis. Proc Natl Acad Sci U S A 104:5354–5359. https://doi.org/10.1073/pnas.0607557104.
19. Smith CA, Antunes NT, Stewart NK, Toth M, Kumarasiri M, Chang M, Mobashery S, Vakulenko SB. 2013. Structural basis for carbapenemase activity of the OXA-23 β-lactamase from *Acinetobacter baumannii*. Chem Biol 20:1107–1115. https://doi.org/10.1016/j.chembiol.2013.07.015.
20. Toth M, Smith CA, Antunes NT, Stewart NK, Maltz L, Vakulenko SB. 2017. The role of conserved surface hydrophobic residues in the carbapenemase activity of the class D β-lactamases. Acta Crystallogr D Struct Biol 73:692–701. https://doi.org/10.1107/S2059798317008671.
21. Lund BA, Thomassen AM, Nesheim BHB, Carlsen TJO, Isaksson J, Christopeit T, Leiros HS. 2018. The biological assembly of OXA-48 reveals a dimer interface with high charge complementarity and very high affinity. FEBS J 285:4214–4228. https://doi.org/10.1111/febs.14643.
22. Liebschner D, Afonine PV, Moriarty NW, Poon BK, Sobolev OV, Terwilliger TC, Adams PD. 2017. Polder maps: improving OMIT maps by excluding bulk-solvent. Acta Crystallogr D Struct Biol 73:148–157. https://doi.org/10.1107/S2059798316018210.
23. Akhter S, Lund BA, Ismael A, Langer M, Isaksson J, Christopeit T, Leiros HS, Bayer A. 2018. A focused fragment library targeting the antibiotic resistance enzyme oxacillinase-48: synthesis, structural evaluation and inhibitor design. Eur J Med Chem 145:634–648. https://doi.org/10.1016/j.ejmech.2017.12.085.
24. Stewart NK, Smith CA, Antunes NT, Toth M, Vakulenko SB. 2018. Role of the hydrophobic bridge in the carbapenemase activity of class D β-lactamases. Antimicrob Agents Chemother 63:e02191-18. https://doi.org/10.1128/AAC.02191-18.
25. Bondi A. 1964. Van der Waals volumes and radii. J Phys Chem 68:441–451. https://doi.org/10.1021/j100785a001.
26. King AM, King DT, French S, Brouillette E, Asli A, Alexander JA, Vuckovic M, Maiti SN, Parr TR, Brown ED, Malouin F, Strynadka NC, Wright GD. 2016. Structural and kinetic characterization of diazabicyclooctanes as dual inhibitors of both serine-β-lactamases and penicillin-binding proteins. ACS Chem Biol 11:864–868. https://doi.org/10.1021/acschembio.5b00944.
27. Stojanoski V, Adamski CJ, Hu L, Mehta SC, Sankaran B, Zwart P, Prasad BV, Palzkill T. 2016. Removal of the side chain at the active-site serine by a glycine substitution increases the stability of a wide range of serine β-lactamases by relieving steric strain. Biochemistry 55:2479–2490. https://doi.org/10.1021/acs.biochem.6b00056.
28. Kabsch W. 2010. XDS. Acta Crystallogr D Biol Crystallogr 66:125–132. https://doi.org/10.1107/S0907444909047337.
29. Evans PR, Murshudov GN. 2013. How good are my data and what is the resolution? Acta Crystallogr D Biol Crystallogr 69:1204–1214. https://doi.org/10.1107/S0907444913000061.
30. Vagin A, Teplyakov A. 1997. MOLREP: an automated program for molecular replacement. J Appl Crystallogr 30:1022–1025. https://doi.org/10.1107/S0021889897006766.
31. King DT, King AM, Lal SM, Wright GD, Strynadka NC. 2015. Molecular mechanism of avibactam-mediated β-lactamase inhibition. ACS Infect Dis 1:175–184. https://doi.org/10.1021/acsinfecdis.5b00007.
32. Emsley P, Cowtan K. 2004. Coot: model-building tools for molecular graphics. Acta Crystallogr D Biol Crystallogr 60:2126–2132. https://doi.org/10.1107/S0907444904019158.
33. Adams PD, Afonine PV, Bunkóczi G, Chen VB, Davis IW, Echols N, Headd JJ, Hung LW, Kapral GJ, Grosse-Kunstleve RW, McCoy AJ, Moriarty NW, Oeffner R, Read RJ, Richardson DC, Richardson JS, Terwilliger TC, Zwart PH. 2010. PHENIX: a comprehensive Python-based system for macromolecular structure solution. Acta Crystallogr D Biol Crystallogr 66:213–221. https://doi.org/10.1107/S0907444909052925.